Journal of The Electrochemical Society, **150** (6) D99-D107 (2003)
0013-4651/2003/150(6)/D99/9/$7.00 © The Electrochemical Society, Inc.

Chlorine Recovery from Anhydrous Hydrogen Chloride in a Molten Salt Electrolyte Membrane Cell

Jessica Bartling[z] and Jack Winnick*

School of Chemical Engineering, Georgia Institute of Technology, Atlanta, Georgia 30332, USA

A novel electrochemical membrane process has been developed to recover chlorine from anhydrous HCl waste. The proposed method produces a pure chlorine product stream and a hydrogen-enriched stream from HCl waste in a single step. The electrochemical method requires only an external electric potential and no concentration gradient, and it produces chlorine with exceptional selectivity. The electrolyzer can be operated at high current densities and current efficiencies. Downstream separation is not necessary, and no exotic electrode materials are required. A single experimental cell was constructed and tested for HCl removal and chlorine production from concentrated HCl reactant streams at variable flow rate. Applied current densities exceeded 400 mA/cm^2, and conversions over 94% were achieved. Ohmic resistance dominated cell potentials due to the formation of hydrogen and chlorine bubbles. The proposed process is found to be a viable option for the treatment of anhydrous HCl waste.
[DOI: 10.1149/1.1568111]

Manuscript submitted July 3, 2002; revised manuscript received December 2, 2002. Available electronically April 10, 2003.

Chlorine is one of the most widely used commodity chemicals, with a world production of approximately 48 million metric tonnes per year.[1] It is a precursor for numerous end products such as polyvinyl chloride (PVC), silicone, and polyurethanes. The chlorine used may appear in the final product, or it may be used only for the production of intermediate products. Most often half of the chlorine used ends up as a reduced species of chloride, typically anhydrous hydrogen chloride (HCl), aqueous hydrochloric acid, or chloride salts.[2]

The formation of HCl as a waste by-product creates serious economic and environmental problems. Although sometimes the waste HCl can be used for making more of the desired product, most chlorination reactions are thermodynamically unfavorable when HCl is substituted as the chlorine source.[2] Alternatively, it can be sold as hydrochloric acid. However, the demand for hydrochloric acid is often not matched with its production as a by-product. Shipping the acid, which is roughly two-thirds water, can be economically prohibitive over long distances. Traditionally, HCl waste has been neutralized with caustic and discharged into wastewater streams, but this environmentally unsound practice is no longer encouraged. Alternatively, the HCl can be converted to chlorine for recycle in chlorination processes. For large-scale manufacturers, recovering the material value of chlorine from HCl is often the most attractive, economic solution.

The growing need to treat HCl waste has prompted several techniques for converting both anhydrous hydrogen chloride and hydrochloric acid to chlorine. Converting HCl to chlorine can be carried out thermochemically or electrochemically. The classical Deacon thermal catalytic oxidation process couples gaseous HCl oxidation with the oxygen reduction reaction in the presence of an inert porous catalyst, resulting in the formation of chlorine and water.[3]

$$2\mathrm{HCl} + 1/2\mathrm{O}_2 \rightarrow \mathrm{Cl}_2 + \mathrm{H}_2\mathrm{O} \qquad [1]$$

In general, thermochemical HCl decomposition is unit operation-intensive, is limited to low single pass conversions, and requires downstream separation due to the production of water vapor.

Alternatively, HCl may be decomposed electrochemically. In the Uhde, or DeNora, electrolysis cell, hydrochloric acid is fed to both the anode and the cathode, and direct current is used to decompose HCl[4,5]

$$2\mathrm{HCl}_{(\mathrm{aq})} \rightarrow \mathrm{H}_2 + \mathrm{Cl}_2 \qquad [2]$$

The reaction may be regarded as two electrode processes, in which protons are reduced at the cathode, while chloride ions are oxidized at the anode.

$$2\mathrm{H}^+ + 2\mathrm{e}^- \rightarrow \mathrm{H}_2 \qquad [3]$$

$$2\mathrm{Cl}^- \rightarrow \mathrm{Cl}_2 + 2\mathrm{e}^- \qquad [4]$$

The technology utilizes a diaphragm to separate the electrodes by a few millimeters, thus producing separate hydrogen and chlorine streams. Today, Bayer and Hoechst operate aqueous HCl electrolyzers based on the Uhde finite gap technology.

General Electric took a different approach to operating the De Nora electrolyzer by employing solid polymer electrolyte technology.[6] In place of the spatially separate anode, cathode, and diaphragm cell separator used in the conventional Uhde cell, the GE/De Nora Genor system utilizes a single structure in which catalytic electrodes are directly bonded to an ion exchange membrane cell separator. In the Genor process, aqueous HCl electrolyte is fed to the anode, while no external liquid is supplied to the cathode. Hydrogen chloride is oxidized at the anode to form chlorine. The Nafion perfluorosulfonic acid polymer, developed by DuPont, serves as an electrolyte membrane, which selectively transports protons (H^+) to the cathode where they are reduced to form hydrogen.

One drawback to this method is the production of wet chlorine gas that requires downstream separation. Another problem is the potentially parasitic oxygen evolution reaction that can take place at the anode at low chloride concentrations or high current densities. DuPont recently sought to improve the process by producing essentially dry chlorine gas in a polymer electrolyte membrane cell.[2,7,8,9] The process allows for direct processing of anhydrous hydrogen chloride, rather than hydrochloric acid, thus eliminating the need for downstream separation of water from the chlorine gas. The method also circumvents the production of oxygen at the anode. Another advantage of using anhydrous hydrogen chloride is that the theoretical cell voltage is lower by at least 300 mV, compared to that of aqueous hydrogen chloride.

In the DuPont process, anhydrous hydrogen chloride is directly oxidized to form chlorine gas and protons at the anode

$$2\mathrm{HCl}_{(\mathrm{g})} \rightarrow 2\mathrm{H}^+ + \mathrm{Cl}_2 + 2\mathrm{e}^- \qquad [5]$$

A Nafion membrane serves as the electrolyte in which protons carry the current. Protons produced at the anode are transported under an electric potential gradient to the cathode. In one envisioned mode, water is fed to the cathode to hydrate the membrane and thereby enhance proton transport. Protons are reduced at the cathode, and the evolved hydrogen bubbles through the water and exits through the cathode outlet.

---

* Electrochemical Society Active Member.

[z] E-mail: jessica.bartling@che.gatech.edu

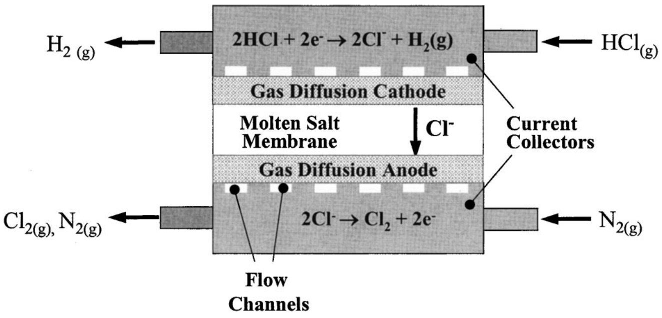

Figure 1. Production of chlorine from anhydrous hydrogen chloride in a molten salt electrolyte membrane cell.

Scientists at Kyoto University developed an electrochemical method to convert anhydrous HCl to chlorine by employing a molten salt electrolyte.[10] The use of a molten salt electrolyte offers advantages over other chlorine recovery methods. It minimizes corrosion and large overvoltages associated with aqueous electrochemical systems. Since the theoretical HCl decomposition voltage is lower than that of aqueous hydrochloric acid, the molten salt system appears advantageous from a thermodynamic viewpoint. Furthermore, operating at higher temperatures enhances electrolyte conductivity.

A novel method involving the reduction, rather than the oxidation, of HCl was proposed.[10] Anhydrous hydrogen chloride is fed to a gas-diffusion porous carbon cathode. Both the cathode and a graphite anode are immersed in a molten salt eutectic mixture of lithium chloride (58 mol %) and potassium chloride (42 mol %) at 400°C. Gaseous hydrogen chloride is fed to the cathode, where it is directly decomposed to form hydrogen gas and chloride ions

$$2HCl_{(g)} + 2e^- \rightarrow H_2 + 2Cl^- \qquad [6]$$

The chloride ions are simultaneously oxidized at the anode to form chlorine

$$2Cl^- \rightarrow Cl_2 + 2e^- \qquad [4]$$

It would seem, therefore, advantageous to combine the molten salt electrolyte chemistry with the membrane separation technology.

Theory

Proposed process.—The process described exploits the chemistry of the Kyoto University method but utilizes a chloride-conducting membrane. The result is a simple process, capable of producing pure chlorine in a single step. Figure 1 shows a schematic of the proposed electrochemical chlorine recovery cell.

Anhydrous hydrogen chloride is fed to the cell through an electrically conductive cell housing. The gas diffuses through a porous cathode to the interface between the cathode and the electrolyte membrane. Current is applied to the cell, and HCl is reduced at the cathode/electrolyte interface under applied current to produce hydrogen gas and chloride ions

$$2HCl_{(g)} + 2e^- \rightarrow H_2 + 2Cl^- \qquad [6]$$

The molten salt electrolyte is entrained in an inert porous ceramic membrane situated between the gas-diffusion electrodes. The membrane provides a medium for chloride ion transport from the cathode to the anode and a wet seal to prevent gas leakage, while preventing products formed at the two electrodes from mixing. The separator also prohibits physical contact between the anode and cathode, or electrical shorting. Capillary forces draw some of the electrolyte into the pores of the electrode, wetting it with a thin electrolyte film. A highly wetted electrode is desirable since it is at this electrolyte interface where electrochemical reaction occurs.

Table I. Reaction standard potentials at 300°C.

Reaction	ΔG° (kJ/mol)[14]	E° (V)
$2HCl \rightarrow H_2 + Cl_2$	195.62	−1.01
$H_2O \rightarrow H_2 + \frac{1}{2} O_2$	215.11	−1.11
$2H_2O + 2LiCl \rightarrow H_2 + 2LiOH + Cl_2$	358.18	−1.86
$2H_2O + 2KCl \rightarrow H_2 + 2KOH + Cl_2$	502.60	−2.60
$2H_2O + 2CsCl \rightarrow H_2 + 2CsOH + Cl_2$	534.62	−2.77
$2LiCl \rightarrow 2Li^\circ + Cl_2$	709.20	−3.68
$2KCl \rightarrow 2K^\circ + Cl_2$	741.88	−3.84
$2CsCl \rightarrow 2Cs^\circ + Cl_2$	761.16	−3.94

The hydrogen is relatively insoluble in the molten salt electrolyte and therefore exits through the cathode. The chloride ions migrate across the electrolyte-saturated membrane under an electric potential gradient to the anode where chlorine gas is evolved by oxidation.

$$2Cl^- \rightarrow Cl_2 + 2e^- \qquad [4]$$

The chlorine diffuses through the porous anode, and an inert stream removes the gas through the anodic housing. The overall reaction results in the decomposition of hydrogen chloride into hydrogen and chlorine

$$2HCl_{(g)} \rightarrow H_2 + Cl_2 \qquad [7]$$

Electrochemical membrane gas separation.—The separation of uncharged species in a typical membrane process is driven by a chemical potential gradient, $\Delta\mu$

$$\Delta\mu_i = \mu_i - \mu_i' = RT \ln(a_i/a_i') \qquad [8]$$

Here, a_i denotes the activity of species i in the contaminated phase and a_i' represents that in the extracted phase. Usually a large concentration gradient or pressure difference, typically several hundred pounds per square inch, is required for mass transfer across the membrane. Conventional membrane separation does not produce a high-purity product, nor does it remove one component with perfect selectivity.

If the component to be removed is the strongest Lewis acid (electron acceptor) in a gas mixture, as is the case with the proposed HCl process, the component can be ionized into an electrolyte. Thus an electrochemical potential gradient can provide the driving force for the charged species across the membrane[11]

$$\Delta\bar{\mu} = \bar{\mu}_i - \bar{\mu}_i' = RT \ln\left(\frac{a_i}{a_i'}\right) + z_i F \Delta\phi \qquad [9]$$

where $\Delta\phi$ represents the applied electric potential, z_i is the charge on species i, and F is Faraday's constant, or the quantity of charge passed per mole of species reduced or oxidized. The electrochemical membrane method requires only an external electric potential and no pressure or concentration gradient. Moreover, it can actually overcome an adverse concentration gradient. Electrochemical membrane separation can produce selectivity considerably higher than that of chemical membrane separations because the electric potential difference affects only the charged species. It has been demonstrated, for example, in the recovery of bromine from hydrogen bromide.[12,13]

Theoretical potentials.—Waste streams from industrial chlorination processes typically contain very high concentrations of HCl. However, these streams may be contaminated by water vapor and possibly organic compounds. Reactions likely to compete with the decomposition of HCl include the direct decomposition of water or the molten salt electrolyte and the decomposition of various organic compounds. Table I compares the decomposition potentials of HCl and some possible parasitic reactions at 300°C.[14] Figure 2 demonstrates the electrochemical window by representing the potential of

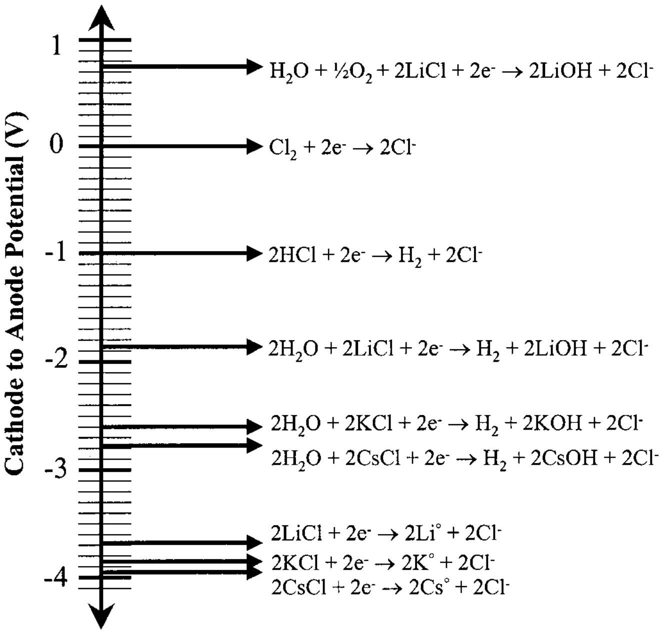

Figure 2. Standard potential window.

each possible half-cell reduction reaction at the cathode versus chlorine evolution, the only oxidation reaction occurring at the anode. Here the potential value of each half-cell reduction reaction is merely a hypothetical one calculated using thermochemical data of single salts. Based solely on the calculated standard potentials, parasitic reactions are not expected to hinder process performance. Only significant amounts of water in the system could potentially threaten process current efficiency. In the absence of water, a high degree of selectivity is likely.

In the proposed cell, the equilibrium potential for the overall decomposition of HCl to form hydrogen and chlorine is provided by the Nernst equation

$$E_{eq} = E^\circ - \frac{RT}{2F}\ln\left(\frac{P_{H_{2(ca)}}P_{Cl_{2(an)}}}{P^2_{HCl_{(ca)}}}\right) \quad [10]$$

where P represents the partial pressures of gaseous reaction species, and E° is the standard potential of HCl reduction versus chloride ion oxidation, near 1.0 V. It is assumed that the activities of the chloride ion at the anode and cathode are equal and diffusion of chloride ions across the electrolyte does not occur. Current flow through the electrolyte is attributed exclusively to the migration of chloride ions. The calculated Nernst potential is plotted *vs.* HCl conversion at 300°C in Fig. 3.

Total cell potential.—The Nernst equation is only strictly true for the special case of equilibrium; it provides no information on the overall reaction rate. The progress of an electrochemical reaction will demand adequate rates of reactant supply to the electrode surface and product removal from it, in addition to charge transfer at the electrode/electrolyte interface. The rate of the overall process will be determined by the slowest of the three steps.

In addition to the Nernst equilibrium potential, electrochemical systems require additional potential necessary to overcome a series of irreversible losses, which occur due to activation barriers with respect to electron transfer, mass transfer limitations of electroactive species, and internal resistances. The equilibrium potential, activation overpotential (η_{act}), concentration overpotential (η_{conc}), and ohmic polarization (IR_{cell}) terms are summed to give the total cross-cell potential required to induce chemical reaction[15]

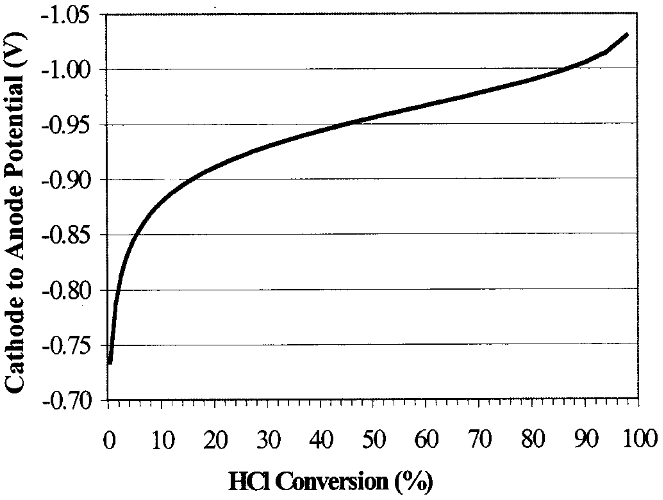

Figure 3. Nernst potential for HCl decomposition at 300°C.

$$E_{cell} = E_{eq} + |\eta_{act}| + |\eta_{conc}| + IR_{cell} \quad [11]$$

It has been determined that electrochemical kinetics do not limit HCl removal process efficiency.[16] Here consideration is given to possible limitations arising from mass transport mechanisms.

Concentration overpotential.—At steady state, the overall rate of a process consisting of a series of steps is determined by its slowest step: electrode kinetics; transport away from the electrode; or, in this case, transport to the electrode. In the proposed electrochemical cell, which involves the use of gas-diffusion electrodes and an electrolyte-saturated membrane, the conversion of HCl proceeds through a series of distinct mass transfer steps. These steps, as illustrated in Fig. 4, are:

1. Gas-phase diffusion of HCl from the bulk stream to the electrode surface
2. Gas-phase diffusion of HCl in the electrode pores
3. Liquid-phase diffusion of HCl through a thin film of electrolyte coating the electrode pores
4. Migration of chloride ions across the electrolyte-saturated membrane
5. Liquid-phase diffusion of chlorine through a thin film of electrolyte coating the electrode pores
6. Gas-phase diffusion of chlorine through the electrode pores, and
7. Gas-phase diffusion of chlorine from the electrode surface to the bulk sweep stream.

The concentration polarization is the additional voltage required due to mass transport limitations[17]

$$\eta_{conc} = \frac{RT}{nF}\ln\left(\frac{i_L - i}{i_L}\right) \quad [12]$$

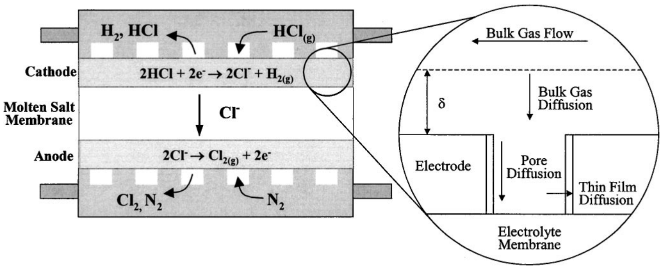

Figure 4. Possible mass transfer limiting steps.

Here, i_L represents the mass transfer limiting current density. Predicted experimental limiting current densities are presented for the transport of reactant HCl to the electroactive area and for the migration of chloride ions across the membrane.

Bulk diffusion.—In the experimental cell, rectangular channels facilitate the flow of reactants and products to and from the electrodes. The Nernst diffusion layer model is used to characterize convection and diffusion of gas-phase reactants to the electrode surface. This simplified model assumes that close to the electrode surface, there exists a totally stagnant mass transfer gas layer of thickness δ, through which diffusion is the only mode of mass transport; outside this layer convection occurs. The current density can be expressed as

$$i = \frac{nFD_{\mathrm{HCl}}(c_{\mathrm{HCl}_{(\mathrm{bulk})}} - c_{\mathrm{HCl}_{(x=0)}})}{\delta} \qquad [13]$$

where D_{HCl} represents the diffusion coefficient of HCl in the gas stream, $(c_{\mathrm{HCl}})_{\mathrm{bulk}}$ is the concentration of HCl in the bulk feed stream, and $(c_{\mathrm{HCl}})_{x=0}$ is the HCl concentration at the electrode. Although the concept of the diffusion layer is widely used, the value of δ is usually unknown. Alternatively, the current density for HCl reduction in terms of diffusion of HCl inside a flow channel from the bulk to the electrode surface is given by

$$i = nFk_m(c_{\mathrm{HCl}_{(\mathrm{bulk})}} - c_{\mathrm{HCl}_{(x=0)}}) \qquad [14]$$

where k_m is the mass transfer coefficient. When the HCl concentration at the electrode surface is equal to zero, HCl is supplied to the electrode at a maximum rate. Therefore the limiting current density under bulk diffusion control is

$$i_{\mathrm{L,bulk}} = nFk_m c_{\mathrm{HC1}_{(\mathrm{bulk})}} = nFk_m\rho \frac{(y_{\mathrm{in}} - y_{\mathrm{out}})}{\ln\left(\frac{y_{\mathrm{in}}}{y_{\mathrm{out}}}\right)} \qquad [15]$$

where a log-mean average of the inlet and outlet concentrations is used to estimate the concentration of HCl in the bulk. The mass transfer coefficient can be determined from the Sherwood number, *Sh*, taken to be 4.11 for laminar flow through the rectangular flow channels used in the experimental cell[18]

$$k_m = \frac{ShD_{\mathrm{HC1}}}{d_{\mathrm{eq}}} \qquad [16]$$

where D_{HCl} is the diffusivity of HCl in the gas mixture and d_{eq} is the equivalent diameter, or characteristic length, of the flow channel. For a rectangular cross section, d_{eq} is given by

$$d_{\mathrm{eq}} = \frac{2ab}{a + b} \qquad [17]$$

where a and b are the depth and width of the flow channel. The equivalent diameter of the flow channels used in the experimental cell is 1.0 mm.

In the absence of experimental data, the diffusivity of HCl in a nitrogen gas stream can be calculated from the Chapman-Enskog equation

$$D_{\mathrm{AB}} = \frac{1.86 \times 10^{-3} T^{3/2}\left(\frac{1}{M_{\mathrm{A}}} + \frac{1}{M_{\mathrm{B}}}\right)^{1/2}}{P\sigma^2_{\mathrm{AB}}\Omega} \qquad [18]$$

where $\mathrm{M_A}$ and $\mathrm{M_B}$ are molecular weights, σ_{AB} is the collision diameter, and Ω is the collision integral of the Lennard-Jones potential.[19] At 300°C, the limiting current density, based on an average molar HCl concentration of 10%, was determined to be 8.9 A/cm^2.

Pore diffusion.—In the proposed cell, electroactive species diffuse through porous three-dimensional (3-D) electrodes to the electroactive area. These gas-diffusion electrodes demonstrate enhanced performance due to their mass transfer characteristics and a high area per unit electrode volume, A_e. The limiting current based on HCl diffusion through the porous cathode is given by

$$I_{\mathrm{L(pore)}} = nFA_eV_ek_mc_{\mathrm{HC1}} \qquad [19]$$

where V_e is the volume occupied by the electrode. By comparison, the limiting current of a 2-D electrode is

$$I_{\mathrm{L}} = nFAk_mc_{\mathrm{HC1}} \qquad [20]$$

The enhanced performance may be expressed as a ratio of the limiting currents, which may exceed a factor of one hundred.[20]

$$\beta = \frac{I_{\mathrm{L(pore)}}}{I_{\mathrm{L}}} = \frac{A_eV_e}{A} \qquad [21]$$

For HCl transport through the porous cathode, an effective diffusion coefficient is defined to describe the average diffusion through the electrode[19]

$$D_{\mathrm{eff}} = \frac{D_{\mathrm{HC1}}\varepsilon_e}{\tau_e} \qquad [22]$$

Here ε_e represents the electrode porosity, and τ_e is its tortuosity. The limiting current for diffusion through the electrode pores can therefore be determined using Eq. 23.

$$i_{\mathrm{L,pore}} = \frac{nFD_{\mathrm{HC1}}\varepsilon}{\tau\delta}c_{\mathrm{HC1}} \qquad [23]$$

Employing a 95% porous electrode with a tortuosity of 2 and thickness of 0.30 mm, the limiting current density, based on an average molar HCl concentration of 10%, is 3.6 A/cm^2.

Thin film diffusion.—Ideally a thin coating of electrolyte wets the walls of the electrode pores, thus increasing the available electroactive area. To maximize this area, the electrode pores should be partially coated, but not entirely flooded, with electrolyte. When the rate of the electrode process is determined by diffusion of dissolved HCl through the thin electrolyte film, the limiting current density, based on the actual reactive surface area along the pore walls, is described by

$$i_{\mathrm{L,film}} = \frac{nFD_{\mathrm{HC1}}}{\delta_{\mathrm{film}}}c_{\mathrm{HC1}} \qquad [24]$$

The HCl diffusion coefficient (D_{HC1}) in molten LiCl-KCl electrolyte has been experimentally determined to be on the order of 10^{-4} cm^2/s in the temperature range 677-793 K.[21] While the electrolyte film thickness, denoted by δ_{film}, is generally unknown, early thin film models for the molten carbonate fuel cell postulated films 0.1 to 0.5 μm thick. Later Mitteldorf and Wilemski estimated carbonate film thicknesses of 30 Å.[22] Assuming a conservative electrolyte film thickness of 0.1 μm, and extrapolating literature HCl solubility data in the binary electrolyte system,[21] the predicted limiting current density is 1.6 A/cm^2.

Membrane migration.—The limiting current density for the migration of chloride ions through the molten electrolyte membrane is given by Eq. 25

$$i_{\mathrm{L,mig}} = \kappa_{\mathrm{eff}}\nabla\Phi \qquad [25]$$

where κ_{eff} represents the effective conductivity of the electrolyte membrane and $\nabla\Phi$ represents the electric potential gradient across the membrane.[23] Analogous to the effective diffusion coefficient in

Table II. Estimated mass transfer limiting current densities.

HCl mass transfer step	i_L (A/cm^2)
Bulk diffusion	8.9
Pore diffusion	3.6
Thin film diffusion	1.6
Membrane migration[a]	1.7

[a] Achievable current density per applied volt.

Eq. 22, effective conductivity is defined as a function of the molten salt electrolyte conductivity (κ), membrane porosity (ε_m) and tortuosity (τ_m).

$$\kappa_{eff} = \frac{\kappa \varepsilon_m}{\tau_m} \quad [26]$$

The conductivity of the molten salt mixture at 573 K (0.767 S/cm) was estimated using data for the binary system LiCl-KCl (59-41 mol %).[24] The system, consisting of a 65% porous membrane with a thickness of 1.0 mm and a tortuosity of 3, is capable of achieving up to 1.7 A/cm^2 per applied volt.

Table II summarizes the predicted limiting current densities dictated by mass transfer control in the experimental separation cell. Based on these calculations, it is predicted that mass transfer will not limit HCl conversion to current densities over 1 A/cm^2.

Experimental

Hydrogen chloride removal was tested for the first time in a single electrochemical membrane cell to experimentally verify the concept. Experiments were initially based on bromine recovery trials conducted in this laboratory, with the implementation of optimized materials as established in the previous tests.[25] Process performance was characterized by HCl removal efficiency, chlorine production and purity, polarization data, and cell longevity. Material compatibility aspects were closely examined.

The single-cell design is shown in Fig. 5. Two electrically conductive half-cell housings directed the flow of current and gas-phase reactants and products to and from the electrodes. A woven mat of (8% yttria-stabilized) zirconia with a thickness of 1 mm and an estimated porosity of 65% was fabricated by Zircar Products and used as a nonconductive, chemically, and thermally stable membrane to absorb the molten salt electrolyte and separate the electrodes. The electrolyte was a eutectic mixture of lithium chloride (57.5 mol %), potassium chloride (13.3%), and cesium chloride (29.2%) with a reported melting temperature of 265°C. Due to their hygroscopic nature, the reagent grade salts (Sigma Chemical) were mixed in a nitrogen environment inside a glove box. The membrane was then presaturated with the electrolyte in a separate furnace by heating it to 350-400°C under a nitrogen purge for a minimum of 4 h to remove residual moisture. The electrolyte/membrane was then cooled and incorporated into the cell at 150°C between the anode and cathode, which were oriented between the faces of the housings. The system was gradually heated to an operating temperature of 315-330°C in an electrically-heated Lindberg furnace. When the electrolyte became molten, weight was applied to the top of the cell using a pneumatic piston. This provided a wet electrolyte seal around the lips of the housings to prevent gas leakage.

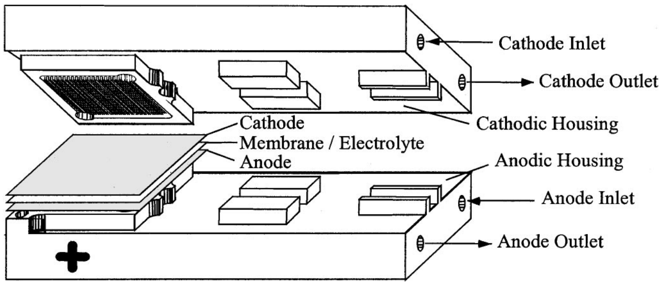

Figure 5. Experimental single cell (Wauters[25]).

Half-cell housings, which must be electrically conductive, chemically resistant, and thermally stable, were fabricated by The Electrosynthesis Co. Housings were machined from graphite and impregnated with glassy carbon to minimize porosity and enhance chemical and thermal stability. 3-D porous electrodes were chosen to provide a high surface area for the electrode reactions involving three-phase contact. Pressed graphite felt ($A = 14.5$ cm^2; Electrosynthesis Co.) and porous carbon aerogel paper ($A = 11.9$ cm^2; Marketech International) were chosen as the gas-diffusion electrodes due to their physical, mechanical, and chemical stability.

Data collection began when the electrolyte became molten and the lips of the housings were sufficiently sealed to permit gas flow through the system. A concentrated mixture of anhydrous HCl in nitrogen, ranging from 25 to 50% HCl (Matheson), was fed to the cathode through an alumina tube at flow rates of 100 to 300 mL/min. Flowmeters equipped with Viton O-rings and tantalum and sapphire beads (Brooks Instrument) were used to measure the flow rates of the HCl-containing streams. As needed throughout the trial, small amounts of electrolyte were fed to the membrane *in situ* through a glass pipette to make up for losses due to incomplete sealing at the cell edges.

A Princeton Applied Research model 371 potentiostat supplied direct current to the cathode. At each applied current, Simpson model 460 multimeters monitored the applied current, anode-to-cathode cross-cell voltage, and electrode potentials *vs.* a graphite rod (0.125 in. diam. POCO Graphite Inc) pseudoreference electrode. Cell ohmic resistance was determined at each current by applying the current interrupt technique and analyzing the output on a Tektronix model 5111A storage oscilloscope. The cathode outlet stream, containing hydrogen and unreacted HCl, was analyzed using Fourier transform infrared spectroscopy (FTIR). Teflon tubing that directed the outlet gas to the FTIR was wrapped in heating tape to maintain the stream at 100°C. The absorbance spectrum generated by the HCl dipole moment was easily identified using a Perkin Elmer FTIR Paragon 500 with a 10 cm path glass cell and calcium fluoride windows. To quantify HCl concentration, the absorbance of the strongest peak at 2944 cm^{-1} was recorded at 5-10 min intervals throughout each trial. FTIR calibration curves were constructed at known HCl concentrations. A second order fit to the data provided the concentration relationship.

Chlorine generated at the anode was removed with a continuous high purity nitrogen purge (Air Products) and occasionally indicated using starch-iodide paper, a common Cl_2 detection technique.[1] The chlorine was condensed with a liquid nitrogen bath and collected until the experimental run was terminated. Following the trial the captured chlorine was purged through the FTIR unit to identify potential contaminants. Of particular interest was the presence of HCl in the anode outlet, possibly indicating a crack in the membrane.

Results and Discussion

Each experimental cell was operated periodically over the course of several days, with the longest-lasting cell enduring 11 days of intermittent operation; afterwards it was voluntarily terminated. The cell was operated at current densities exceeding 400 mA/cm^2, based on a superficial electrode area. Data were collected over a maximum duration of 225 min.

Hydrogen chloride concentration as a function of applied current is plotted in Fig. 6. Conversion values lie in close agreement with those predicted by Faraday's law, based on a process involving two electrons per mole of chlorine produced. Current efficiencies approached 100% in every case. Using a feed of 25% HCl at 100 mL/min, HCl concentration dropped to less than 2% when current was applied at 96% of the stoichiometric current.

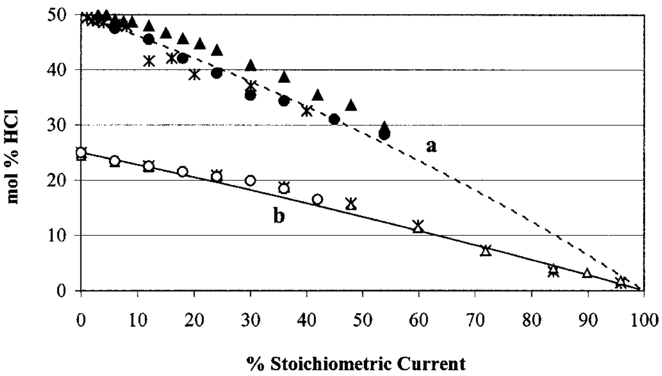

Figure 6. HCl outlet concentration *vs.* applied current. Experimental conversion data and predicted stoichiometric conversion for (a) 50% HCl in nitrogen; (b) 25% HCl in nitrogen.

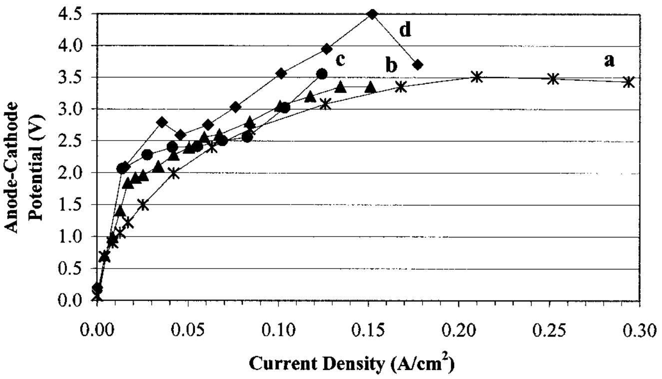

Figure 8. Cross cell potential *vs.* applied current. 50% HCl: (a) 150 ccm, carbon aerogel; (b) 100 ccm, carbon aerogel; (c) 100 ccm, graphite felt; (d) 200 ccm, graphite felt.

Chlorine was immediately detected at the anode at currents as low as 5 mA by a sudden blue coloration of the indicator paper. In each trial no sign of contamination by HCl or other species was observed in the FTIR analysis. The chlorine generated was shown to be pure, down to the lower detection limit of the instrument.

Figure 7 depicts the resulting cross-cell potentials, which have been compensated for ohmic loss, versus applied current density under a cathodic feed of 25% HCl in nitrogen balance. The predicted voltage/current relationship at 325°C based on a gas stream of 25% HCl fed at 100 mL/min is plotted for comparison. Polarization data are shown to be repeatable between runs b and c, which were performed six days apart during the same experimental trial.

Figure 8 shows experimental voltages obtained using a 50% HCl feed stream at varying flow rates. As in Fig. 7, IR-compensated potentials are higher than theoretically predicted and level out around 3.0-3.5 V. Cross-cell potential behavior is shown to be independent of both cathodic inlet flow rate and HCl feed concentration. Since concentration overpotential was not observed, and kinetic limitations were deemed negligible, these effects could not account for the 2 V overpotential.

Ohmic resistance, measured using the current interrupt technique, was higher than anticipated and often exhibited a sharp increase with increasing applied current. The unusual behavior suggests the formation of gas bubbles, hydrogen at the cathode and chlorine at the anode, in the thin films coating the electrode pores. In this regime, small bubbles shroud the electrode surface, thereby increasing the effective cell resistance, and lowering the active electrode area. The Bruggeman equation describes the influence of a gas dispersion on liquid electrolyte conductivity[26]

$$R_{\mathrm{eff}} = R_{\mathrm{o}}(1 - \alpha)^{-1.5} \qquad [27]$$

Here R_{eff} represents the effective resistance, R_{o} is the resistance of the liquid phase, and α is the gas void fraction. It can be seen that even a moderate gas void fraction would increase the resistance dramatically, and because the void fraction is usually a function of current density, the effective liquid phase resistance would increase with current.

Excessive ohmic polarization can also be attributed to contact resistances, which are often exhibited in electrochemical systems during the developmental stages. Systems employing separate gas diffusion electrodes are particularly susceptible to high contact resistance as the highly porous structures make only finite contacts with the conductive cell housings. Additionally, the formation of gas bubbles creates limited point contacts, effectively minimizing the available electrochemically-active area and resulting in high, localized current densities.

Figure 9 demonstrates the half-cell contributions to potential as a function of applied current density for a trial employing carbon aerogel paper as both the anode and cathode. Voltages, recorded *vs.* a graphite pseudoreference electrode, were not compensated for ohmic loss. Current was applied up to the stoichiometric limit for the given feed conditions (5.0 A), which also corresponded to the limit supplied by the instrument. Cross-cell potential is initially dominated by polarization at the cathode. At 300 mA/cm² the potential at the anode exhibits a sudden increase, as the cathodic potential decreases. While in most experiments the cathodic couple was shown to contribute significantly to the total cell potential, in

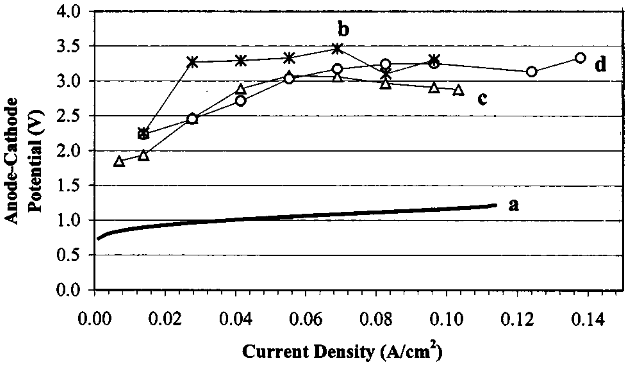

Figure 7. Cross cell potential *vs.* applied current density on graphite felt electrodes with 25% HCl feed: (a) predicted, 100 ccm; (b) 100 ccm; (c) 100 ccm; (d) 200 ccm.

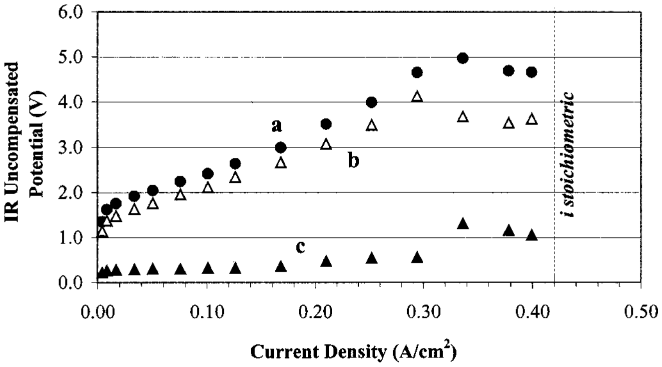

Figure 9. Potential (IR uncompensated) *vs.* applied current density. 25% HCl at 300 mL/min on carbon aerogel: (a) anode cathode; (b) reference cathode; (c) anode reference.

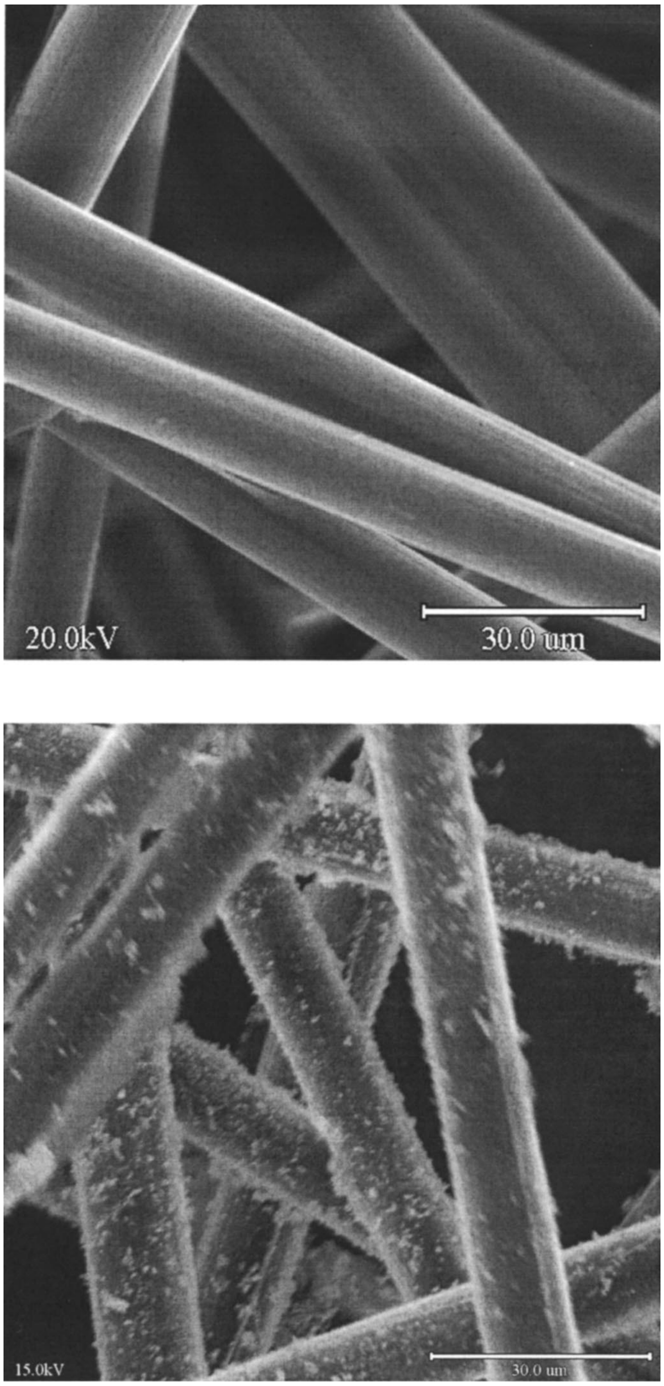

Figure 10. Graphite felt GF-S2 1000 times magnification: (top) pretrial; (bottom) following HCl electrolysis.

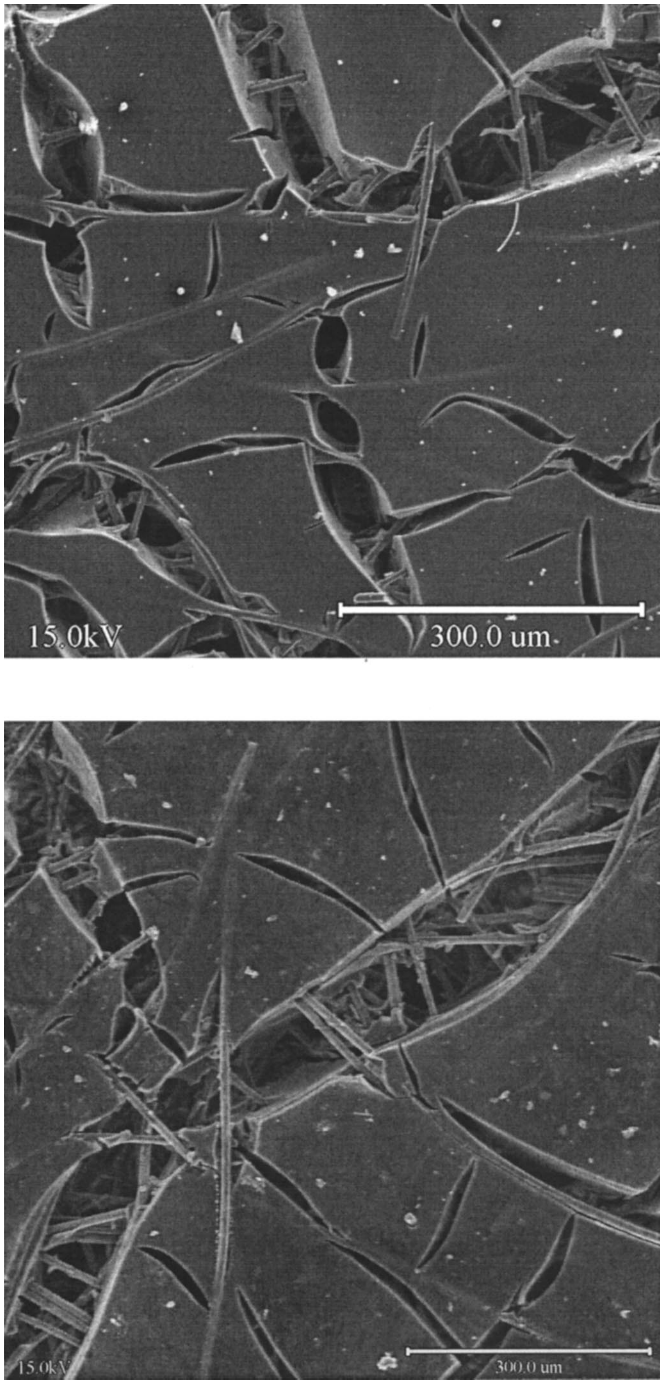

Figure 11. Carbon aerogel 100 times magnification: (top) pretrial; (bottom) following HCl electrolysis.

other trials, the anodic couple dominated. This unusual behavior substantiates the implication that gas bubble formation strongly influenced cell performance.

It is worth noting that during the experiments, the cell experienced several excursions in temperature. The presence of moist air in the cell at low temperatures, combined with the corrosive nature of the HCl, can create a severely adverse environment. An industrial cell would not be intentionally subjected to such a temperature cycling; however, it was of interest in light of process downtime. At one point the temperature was deliberately reduced to ambient (~25°C), and the experiment was later reinitiated. Despite thermal cycling, the cell suffered no loss in performance.

Both graphite felt and carbon aerogel paper performed exceptionally well as gas-diffusion electrodes, offering high electroactive area enhancement. Both electrodes maintained their physical integrity and electrical conductivity despite prolonged cell operation under processing conditions. Scanning electron micrograph (SEM) images of a pressed graphite felt cathode sample before and after a test are presented in Fig. 10. The graphite fibers appear to be coated by residual electrolyte salt; however, they remained completely intact. The physical integrity of the carbon aerogel sample was likewise unaffected. Figure 11 provides an SEM image of a cathode sample before and following a run. The aerogel clearly retained its structure,

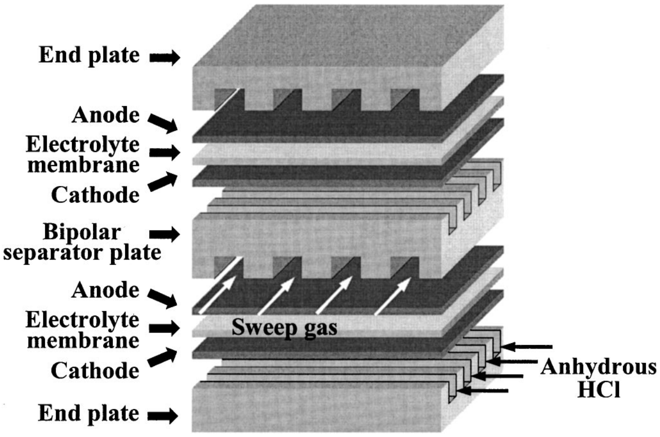

Figure 12. Envisioned commercial design.

while only residual electrolyte is seen to coat the individual graphite fibers.

Economic Feasibility

The envisioned commercial process design, depicted in Fig. 12, is configured as a bipolar array of electrochemical cells. While the ultimate construction and operational costs of the system are impossible to predict at this stage, the material costs for the cell stack can be approximated based on the analogous molten carbonate fuel cell (MCFC), whose material costs are on the order of \$100 per square meter.[27] Since no particularly expensive or exotic materials are required in the proposed chlorine recovery process, capital investment is expected to be lower than that for an equivalent size MCFC plant, where nickel electrodes are employed. The process offers the advantage of *in situ* separation of HCl from the Cl_2 product; thus, the total capital investment would be lower than that of a typical chlor-alkali facility.

Operating costs are determined essentially by the stack's specific energy consumption[20]

$$E_s = -\frac{nFE_{\text{cell}}}{\phi M_{\text{Cl}_2}} \qquad [28]$$

where ϕ represents the process current efficiency. Based on our experimentally observed IR-compensated potential of 3.0 V, 100% HCl removal current efficiency, and an electricity cost of \$0.035/kWh, operating costs are estimated to be \$80/t of Cl_2 produced. With further development, however, operating potentials approaching 1 V are more reasonable; therefore, electricity costs near \$30/t Cl_2 are more realistic, and of course disposal costs for the waste HCl are severely diminished. In April, 2002, chlorine contract prices rose to \$80-\$110 per ton and are predicted to rise for the remainder of 2002 due to strengthening demand.[28]

Conclusions

The production of chlorine from anhydrous hydrogen chloride using an electrochemical molten salt membrane cell is a novel process. It has been tested for the first time in a single electrochemical experimental cell. The single cell trials demonstrate the feasibility of the proposed process for removing HCl from process waste streams and separating it into hydrogen and chlorine. Despite the higher-than-predicted cell voltages, HCl removal efficiencies exceeded 94% at near 100% current efficiency. Chlorine production was immediately indicated at low current density, and FTIR analysis established the purity of chlorine, identifying no contamination by HCl or other species. Experimental cross-cell potentials were reasonable, typically 3.0-3.5 V. The experimental cell was operated at current densities up to 400 mA/cm^2, and it performed over extended periods of time. Temperature cycling did not affect cell performance or longevity. The materials required for the molten salt membrane cell are mundane in nature and relatively inexpensive.

The formation of gas bubbles, hydrogen at the cathode, and chlorine at the anode, greatly influenced cell performance and increased ohmic polarization. In practice, bubble formation is a commonly encountered industrial challenge. With minor design modifications and proper cell operation, the process shows promise for industrial development.

Future work will evaluate single cell performance using gas feed streams characteristic of chlorination processes. Feed conditions will be varied to mimic those of real processes and evaluate for inefficiencies imposed by possible competing reactions. Minimizing the resistance of the electrochemical cell is necessary to reduce the unit-cell voltage and operating costs. Fundamental studies will be undertaken to elucidate the source of overpotential.

Acknowledgment

Financial support of this research was provided by the DuPont Corporation, Inc. The authors would like to acknowledge Marketech International for donating samples of the carbon aerogel papers. The authors express their sincere appreciation to Dr. Cary Wauters for his technical guidance.

List of Symbols

A	area, cm^2
A_e	area per unit electrode volume, cm^{-1}
a_i	activity of species i in the contaminated phase
a_i'	activity of species i in the extracted phase
a	depth of the flow channel, cm
b	width of the flow channel, cm
c	concentration of HCl in the gas or liquid phase, mole cm^{-3}
D_{HCl}	diffusivity of HCl in the gas or liquid phase, cm^2 s^{-1}
D_{eff}	effective diffusivity, cm^2 s^{-1}
d_{eq}	equivalent diameter, cm
E°	standard potential, V
E_{eq}	equilibrium Nernst potential, V
E_{cell}	cross-cell potential, V
F	Faraday's constant, 96485 C mol^{-1}
I	current, A
I	current density, A cm^{-2}
i_L	mass transfer limiting current density, A cm^{-2}
k_m	mass transfer coefficient, cm s^{-1}
M_i	molecular weight of species i, g mol^{-1}
n	number of electrons transferred
P_i	partial pressure of gaseous reaction species i, atm
R	gas constant, 8.314 J mol^{-1} K^{-1}
R_{cell}	resistance across the cell (ohm)
R_{eff}	effective resistance (ohm)
R_o	liquid-phase resistance (ohm)
Sh	Sherwood number
T	temperature (K)
V_e	electrode volume (cm^3)
y_{in}	mole fraction of HCl in inlet gas
y_{out}	mole fraction of HCl in outlet gas
z_i	charge on species i

Greek

α	gas void fraction
β	area enhancement factor
δ	diffusion layer thickness, cm
δ_{film}	electrolyte film thickness, cm
ε_e	electrode porosity
ε_m	membrane porosity
ϕ	applied electric potential, V
ϕ	current efficiency
$\nabla\Phi$	electric potential gradient, V cm^{-1}
η_{act}	activation overpotential, V
η_{conc}	concentration overpotential, V
κ	electrical conductivity, Ω^{-1} cm^{-1}
κ_{eff}	effective electrical conductivity, Ω^{-1} cm^{-1}
μ_i	chemical potential of species i in contaminated phase, J mol^{-1}
μ_i'	chemical potential of species i in extracted phase, J mol^{-1}
$\Delta\mu_i$	chemical potential gradient of species i, J mol^{-1}
$\overline{\mu_i}$	electrochemical potential of species i in contaminated phase, J mol^{-1}
$\overline{\mu_i'}$	electrochemical potential of species i in extracted phase, J mol^{-1}
$\Delta\overline{\mu_i}$	electrochemical potential gradient of species i, J mol^{-1}
ρ	density of gas, mol cm^{-3}

σ_{AB} collision diameter, Å
τ_e electrode tortuosity
τ_m membrane tortuosity
Ω collision integral

References

1. *Chlorine: Principles and Industrial Practice*, P. Schmittinger, Editor, p. 223, Wiley-VCH, Weinheim, Germany (2000).
2. S. Motupally, D. T. Mah, F. J. Freire, and J. W. Weidner, *Electrochem. Soc. Interface*, **7**, 32 (1998).
3. H. Deacon, U.S. Pat. 85,370 (1868).
4. S. Payer, *Hydrocarbon Process.*, **53**, 147 (1974).
5. P. Gallone and G. Messner, *Electrochem. Technol.* , **3**, 321 (1965).
6. E. N. Balko, J. F. McElroy, and A. B. LaConti, *Int. J. Hydrogen Energy*, **6**, 577 (1981).
7. D. J. Eames and J. Newman, *J. Electrochem. Soc.*, **142**, 3619 (1995).
8. J. A. Trainham, C. G. Law, J. S. Newman, K. B. Keating, and D. J. Eames, U.S. Pat. 5,411,641 (1995).
9. J. A. Trainham, C. G. Law, J. S. Newman, K. B. Keating, and D. J. Eames, U.S. Pat. 5,580,437 (1996).
10. S. Yoshizawa, Z. Takehara, Y. Ito, and K. Oka, *J. Appl. Electrochem.*, **1**, 245 (1971).
11. J. Winnick, *Chem. Eng. Prog.* **86**, 41 (1990).
12. C. N. Wauters and J. Winnick, *J. Electrochem. Soc.*, **143**, L184 (1996).
13. C. N. Wauters and J. Winnick, *AIChE J.*, **44**, 2144 (1998).
14. M. W. Chase, C. A. Davies, J. R. Downey, D. J. Frurip, R. A. McDonald, and A. N. Syverud, *J. Phys. Chem. Ref. Data*, **14**, 1 (1985).
15. V. V. Stender, P. B. Zivotinsky, and M. M. Stroganoff, *Trans. Electrochem. Soc.*, **65**, 189 (1934).
16. J. M. Johnson, Ph.D. Thesis, Georgia Institute of Technology, (2001).
17. A. J. Bard and L. R. Faulkner, *Electrochemical Methods*, John Wiley & Sons, New York (1980).
18. W. M. Kays, *Convective Heat and Mass Transfer*, McGraw-Hill, New York (1966).
19. E. L. Cussler, *Diffusion Mass Transfer in Fluid Systems*, 2nd ed., Cambridge University Press, Cambridge, U.K. (1997).
20. F. C. Walsh, *A First Course in Electrochemical Engineering*, p. 142, The Electrochemical Consultancy, Alresford Press Ltd., Alresford, Hants, U.K. (1993).
21. N. Q. Minh and B. J. Welch, *Aust. J. Chem.*, **28**, 965 (1975).
22. J. Mitteldorf and G. Wilemski, *J. Electrochem. Soc.*, **131**, 1784 (1984).
23. J. S. Newman, *Electrochemical Systems*, p. 340, Prentice-Hall, Inc., Englewood Cliffs, NJ (1973).
24. G. J. Janz, *J. Phys. Chem. Ref. Data*, **17**, 2 (1988).
25. C. N. Wauters, Ph.D. Thesis, Georgia Institute of Technology (1997).
26. C. W. Tobias, *J. Electrochem. Soc.*, **106**, 833 (1959).
27. A. J. Appleby and F. R. Foulkes, *Fuel Cell Handbook*, p. 575, Van Nostrand Reinhold, New York (1989).
28. P. H. Sim, *Chem. Week*, , April 17 (2002).